

UCLA

UCLA Previously Published Works

Title

Comparison of Monophosphine and Bisphosphine Precatalysts for Ni-Catalyzed Suzuki-Miyaura Cross-Coupling: Understanding the Role of the Ligation State in Catalysis.

Permalink

<https://escholarship.org/uc/item/3cx5s7p3>

Journal

ACS Catalysis, 13(12)

ISSN

2155-5435

Authors

Borowski, Julia

Newman-Stonebraker, Samuel

Doyle, Abigail

Publication Date

2023-06-16

DOI

10.1021/acscatal.3c01331

Peer reviewed



# HHS Public Access

Author manuscript

ACS Catal. Author manuscript; available in PMC 2023 November 30.

Published in final edited form as:

ACS Catal. 2023 June 16; 13(12): 7966–7977. doi:10.1021/acscatal.3c01331.

## Comparison of Monophosphine and Bisphosphine Precatalysts for Ni-Catalyzed Suzuki–Miyaura Cross-Coupling: Understanding the Role of the Ligation State in Catalysis

Julia E. Borowski<sup>a</sup>, Samuel H. Newman-Stonebraker<sup>†,a,b</sup>, Abigail G. Doyle<sup>b,\*</sup>

<sup>a</sup>Department of Chemistry, Princeton University, Princeton, NJ 08544

<sup>b</sup>Department of Chemistry and Biochemistry, University of California, Los Angeles, CA 90095

### Abstract

Practical advances in Ni-catalyzed Suzuki–Miyaura cross-coupling (SMC) have been limited by a lack of mechanistic understanding of phosphine ligand effects. While bisphosphines are commonly used in these methodologies, we have observed instances where monophosphines can provide comparable or higher levels of reactivity. Seeking to understand the role of ligation state in catalysis, we performed a head-to-head comparison study of C(sp<sup>2</sup>)–C(sp<sup>2</sup>) Ni SMCs catalyzed by mono and bisphosphine precatalysts using six distinct substrate pairings. Significant variation in optimal precatalyst was observed, with the monophosphine precatalyst tending to outperform the bisphosphines with electronically deactivated and sterically hindered substrates. Mechanistic experiments revealed a role for monoligated (P<sub>1</sub>Ni) species in accelerating the fundamental organometallic steps of the catalytic cycle, while highlighting the need for bisligated (P<sub>2</sub>Ni) species to avoid off-cycle reactivity and catalyst poisoning by heterocyclic motifs. These findings provide guidelines for ligand selection against challenging substrates and future ligand design tailored to the mechanistic demands of Ni-catalyzed SMCs.

### Graphical Abstract

\*Corresponding Author: Abigail G. Doyle, Department of Chemistry and Biochemistry, University of California, Los Angeles, CA; agdoyle@chem.ucla.edu.

<sup>†</sup>Present Addresses: Department of Chemistry, Yale University, New Haven, CT 06511

Julia E. Borowski – Department of Chemistry, Princeton University, Princeton, NJ 08544;

Samuel H. Newman-Stonebraker - Department of Chemistry, Princeton University, Princeton, NJ 08544; Department of Chemistry and Biochemistry, University of California, Los Angeles, CA;

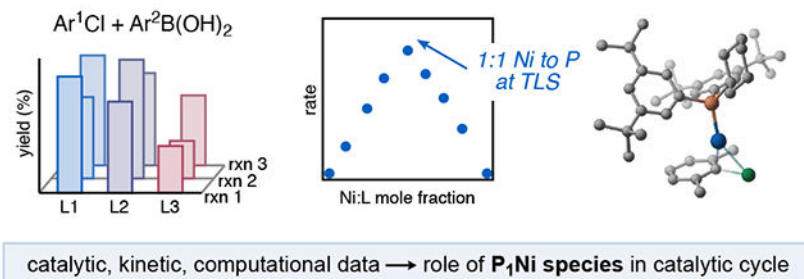
**Supporting Information.** The Supporting Information is available free of charge at <https://pubs.acs.org/>.

Experimental procedures; experimental data; and characterization and spectral data for new compounds (PDF)

XYZ coordinates for DFT-computed structures (ZIP)

Accession Codes

2202065, 2202066, and 2202067 contain the supplementary crystallographic data for this paper. These data can be obtained free of charge via [www.ccdc.cam.ac.uk/data\\_request/cif](http://www.ccdc.cam.ac.uk/data_request/cif), or by emailing [data\\_request@ccdc.cam.ac.uk](mailto:data_request@ccdc.cam.ac.uk), or by contacting The Cambridge Crystallographic Data Centre, 12 Union Road, Cambridge CB2 1EZ, UK; fax: +44 1223 336033.

head-to-head comparison of *monophosphine* and *bisphosphine* Ni precatalysts**Keywords**

Ni catalysis; phosphines; Suzuki-Miyaura; ligand effects; cross-coupling

**INTRODUCTION**

Mechanistically-driven phosphine ligand design for transition metal-catalyzed cross-coupling reactions has enabled the development of robust methodologies for carbon-carbon and carbon-heteroatom bond formation under mild conditions with low catalyst loading.<sup>1,2,3,4</sup> In Suzuki-Miyaura cross-coupling reactions (SMCs), extensive studies of Pd-catalyzed methodologies have identified that unsaturated L<sub>1</sub>Pd intermediates (where L is a monophosphine ligand) are generally necessary to promote the organometallic steps of catalysis.<sup>5,6,7,8</sup> These findings have prompted the design and implementation of electron-rich and sterically-bulky monophosphine ligands to preferentially form L<sub>1</sub>Pd intermediates that promote efficient catalysis while protecting against off-cycle reactivity (Figure 1a).<sup>9,10,11</sup> While this design principle has been highly enabling for Pd, recent efforts to develop analogous Ni-catalyzed methodologies have revealed that these ligand design principles do not necessarily translate between the two metals.<sup>12</sup> Namely, the ligands that are most effective for Pd, including bulky trialkyl (e.g., P(*t*-Bu)<sub>3</sub>, P(Ad)<sub>3</sub>), triaryl (e.g., P(*o*-tol)<sub>3</sub>), and highly-substituted dialkyl-biaryl phosphines (e.g., *t*-BuBrettPhos) are not similarly privileged in Ni-catalyzed SMCs.<sup>13,4,14,15</sup>

By contrast, bisphosphine ligands like 1,1'-bis(diphenylphosphino)ferrocene (dppf) are commonly used in Ni-catalyzed SMCs and have been incorporated into air-stable precatalysts that enable efficient C(sp<sup>2</sup>)-C(sp<sup>2</sup>) bond formation with (hetero)aryl substrates (Figure 1a).<sup>16,17,18</sup> A simple rationalization of the use of bisphosphines over monophosphines in Ni-catalyzed SMCs is that, by virtue of being able to occupy two coordination sites in an entropically-favorable chelate, these ligands can avoid the formation of vacant coordination sites that can enable unproductive reactivity.<sup>13,19,20</sup> Additionally, bulky bisphosphines, like those developed by Stradiotto and coworkers, can facilitate a more facile reductive elimination step.<sup>4</sup>

While these ligands have been enabling for Ni, previous work by our lab in developing the Ni-catalyzed SMC of benzylic acetals revealed an instance where both state-of-the-art bisphosphines and monophosphines were inactive or low-yielding, respectively, in catalysis

(see SI for details).<sup>12,13</sup> Development of a series of monophosphines possessing remote steric bulk, quantified by high values of cone angle and low values of percent buried volume (%  $V_{\text{bur}}$ ), enabled high yields for this transformation (Figure 1b). These ligands, collectively referred to as the DinoPhos ligands, have subsequently been demonstrated by our group and others to be top performers in other Ni-catalyzed SMCs.<sup>21</sup> Seeking to understand the significance of this steric profile in Ni-catalyzed SMCs, we undertook a high-throughput experimentation (HTE) and ligand featurization campaign, in collaboration with the Sigman Laboratory and Merck Sharpe and Dohme. Univariate analysis of reaction yields against ligand steric features revealed a threshold in Ni-catalyzed SMC reactivity as a function of monophosphine minimum percent buried volume (%  $V_{\text{bur}}(\text{min})$ ),<sup>22</sup> wherein yields above those attained under ligand-free conditions were only observed for ligands with values of %  $V_{\text{bur}}(\text{min})$  below ~32%. We observed experimentally that this reactivity threshold is a readout of ligation state, with ligands below the threshold forming  $L_2\text{Ni}(0)$  species and those above forming  $L_1\text{Ni}(0)$ .<sup>13</sup> This analysis demonstrated that successful monophosphines for Ni catalysis must be able to form a bisligated Ni species. Extending our analysis to a series of Pd-catalyzed cross-coupling datasets, we again observed reactivity thresholds with opposite directionality, reflecting higher catalytic performance for monophosphines that form  $L_1\text{Pd}$  species (Figure 1c).

Given our demonstration that bisligated  $L_2\text{Ni}$  is required for reactivity, it is unsurprising that bisphosphines, in addition to monophosphines below the %  $V_{\text{bur}}(\text{min})$  threshold (e.g.,  $\text{PCy}_3$ ), are commonly employed in Ni-catalyzed SMCs.<sup>23,24,25</sup> Interestingly, in our HTE studies, we found that the highest yielding ligands were those with %  $V_{\text{bur}}(\text{min})$  values between 29 and 32%. This region corresponds to an area where ligands spectroscopically observed to form  $L_2$  species were active in both Ni and Pd catalysis (Figure 1c, dotted vertical lines). We hypothesized that this overlap signifies a region where ligands thermodynamically favor  $L_2\text{M}$  but can kinetically form  $L_1\text{M}$  intermediates. Moreover, this would suggest that successful ligands for Ni-catalyzed SMCs must balance these two requirements, potentially to both minimize off-cycle reactivity while accelerating productive chemistry, respectively.

Considering this mechanistic possibility, we sought to compare mono- and bisphosphine performance in Ni-catalyzed SMCs to understand how ligand structure impacts catalyst ligation state and reactivity. For clarity, monoligated  $L_1\text{Ni}$  monophosphine and  $[\kappa^1\text{-L}]\text{Ni}$  bisphosphine complexes will be referred to as  $P_1\text{Ni}$ , while bisligated  $L_2\text{Ni}$  monophosphine and  $[\kappa^2\text{-L}]\text{Ni}$  bisphosphine complexes will be referred to as  $P_2\text{Ni}$ . If successful catalysis requires balancing the need for both  $P_2\text{Ni}$  and  $P_1\text{Ni}$  intermediates, we hypothesized that these two classes of phosphines would have their respective strengths and weaknesses which operate as a function of the specific demands of a given substrate pairing. To this end, we have compared the catalytic outcomes of three Ni precatalysts bearing different phosphine ligands—one monophosphine and two bisphosphines—in a series of Ni-catalyzed SMCs of aryl chlorides and aryl boronic acids. No one ligand was observed to be optimal across each substrate pairing surveyed. Further mechanistic experiments and computational studies enabled rationalization of the catalytic outcomes as a function of the required ligation state at different steps in the catalytic cycle (Figure 1d). Our study implicates  $P_1\text{Ni}$  species in catalysis—including for bisphosphine-ligated Ni—while also demonstrating the

need for  $P_2Ni$  species as a way of minimizing unproductive side reactivity and catalyst poisoning and provides guidance for ligand selection as a function of substrate properties.

## RESULTS

To select representative mono- and bisphosphine ligands, we screened a subset of phosphines in catalysis for two electronically-biased substrate pairings (Figure 2). **Reaction 1** (1-chloro-4-trifluoromethylbenzene and 4-methoxybenzene boronic acid) represents an electronically “matched” case, where the electrophile has an inductively withdrawing trifluoromethyl group ( $CF_3$ ;  $\sigma_p = 0.54$ ) and the nucleophile has an electron-donating methoxy group (OMe;  $\sigma_p = -0.27$ ).<sup>26</sup> By contrast, **reaction 2** features the same functional groups but swapped between electrophilic and nucleophilic partners (4-chloroanisole and 4-trifluoromethylbenzeneboronic acid), which represents an electronically “mismatched” substrate pairing. For both reactions, we observed that CyTyrannoPhos (cyclohexylbis(3,5-di-*tert*-butylphenyl)phosphine) (Figure 2, entry 4) was the highest yielding monophosphine. Similarly, we have previously observed that this ligand was consistently high-yielding across a series of substrate pairings in our HTE evaluation of monophosphines in Ni-catalyzed SMCs (see Supporting Information for details). This ligand is commercially available and can be synthesized in a one-pot, two-step procedure from readily available precursors. For these reasons, it was selected as the representative monophosphine for further study.

In selecting bisphosphines for comparison, we first selected dppf (1,1'-bis(diphenylphosphino)ferrocene) as the representative *cis*-binding ligand (Figure 2, entry 6). While it was not the highest-yielding bisphosphine, we thought it would provide a meaningful comparison to prior studies, given that it is commonly used as a benchmark for the performance of Ni-catalyzed SMCs<sup>27</sup> and in mechanistic studies of Ni-catalyzed cross-coupling.<sup>17,19,28</sup> While dppf was chosen to provide a meaningful benchmark relative to prior studies, we observed that a structurally similar *trans*-binding bisphosphine, dcy pf (1,1'-bis(dicyclohexylphosphino)ferrocene), was a top-performing bisphosphine (Figure 2, entry 7).<sup>29</sup> Though this ligand has received less attention in SMC methodologies or mechanistic studies, it has been shown to surpass the performance of dppf in certain instances.<sup>30,31</sup> By directly comparing these two bisphosphines with a high-performing monophosphine, we sought to gain additional insights into how the distinct speciation of these two classes of ligand affects catalytic efficiency and broaden the scope of mechanistic knowledge for Ni-catalyzed SMCs.

For our comparison study, we opted to use  $L_nNi^{II}(o\text{-tolyl})(Cl)$  precatalysts (**1-3**) for their ease of synthesis, air stability, and defined speciation. These precatalysts have been demonstrated to be viable in Ni-catalyzed SMCs, undergoing activation through transmetalation with excess boronic acid followed by reductive elimination to generate the active  $Ni^0$  intermediate.<sup>13c,32,33</sup> Further, the use of this precatalyst platform obviates the need for air- and temperature-sensitive  $Ni(COD)_2$ .

Both  $(dcy pf)Ni^{II}(o\text{-tolyl})(Cl)$  (**2**) and  $(dppf)Ni^{II}(o\text{-tolyl})(Cl)$  (**3**) were synthesized according to literature procedures disclosed by Jamison and coworkers.<sup>16</sup> Structural characterization of these compounds demonstrates the contrasting *cis* and *trans* binding of the dppf

and dcyfp complexes, respectively. With a larger bite angle (dcyfp: 144.0°; dppf: 102.0°) and higher percent buried volume (%  $V_{\text{bur}}$ ) (dcyfp: 59.8%; dppf: 56.7%) relative to dppf, we hypothesized that dcyfp would be more labile in catalysis and represent an intermediate point of comparison between *cis*-binding dppf and the monophosphine, CyTyrannoPhos.<sup>34,35</sup> We successfully synthesized and isolated the corresponding CyTyrannoPhos<sub>2</sub>Ni<sup>II</sup>(*o*-tolyl)(Cl) precatalyst (**1**) for use in the catalytic reactions as the representative monophosphine (Scheme 1).<sup>16</sup>

The full set of substrate pairings were chosen to incorporate functionalities that would provide a readout of ligand performance in different catalytic scenarios (Figure 3c). **Reactions 1** and **2** were revisited with the precatalysts to represent electronically-biased substrate pairings. Similarly, **reaction 3** (4-chloroanisole and 4-ethoxycarbonylphenylboronic acid) has a similarly “mismatched” electronic profile ( $\sigma_{\text{p}}(\text{CO}_2\text{Et}) = 0.45$ ),<sup>26</sup> but also features an ester functionality that can coordinate to Ni<sup>0</sup> catalyst intermediates. Previous reports of Ni-catalyzed SMCs have demonstrated that substrates containing ester functional groups are lower yielding in catalysis<sup>21, 27</sup>. **Reactions 4** (2-chloro-*meta*-xylene and 4-fluoro-phenylboronic acid) and **5** (1-chloro-4-fluorobenzene and 2,4,6-trimethylphenylboronic acid) feature di-*ortho* substitution on the electrophile and nucleophile that we hypothesized would have slow oxidative addition and transmetalation steps, respectively, that affect the overall efficiency of catalysis and flux of catalytic intermediates. Lastly, **reaction 6** (3-chloropyridine and 2-thienylboronic acid) was chosen to include synthetically relevant heterocyclic motifs, which can be catalytically challenging with Ni due to catalyst poisoning and relatively higher rates of nucleophile protodeboronation competing with productive chemistry.

Each substrate pairing was tested against all three precatalysts from a common set of conditions, with minimal alterations made to facilitate sufficient yields for meaningful comparisons (Figure 3a). Yields were determined at two time points: (1) the time at which the highest yielding catalyst either reaches ~90% yield or stalls, as indicated for each reaction in Figure 3c, and (2) 24 hours. The second timepoint enabled us to differentiate between cases where one catalyst system was slower in forming product and those where one catalyst became inactive over the course of the reaction. The substrate pairings and yields, depicted graphically, are shown in Figure 3c.

As expected, given the electronically activated coupling partners, **reaction 1** was high yielding for each precatalyst with a relatively short reaction time (6 h), confirming that these catalysts were competent under these reaction conditions. However, when the substituents were flipped (**reaction 2**), deactivating both substrates, **1** was the highest yielding (88%) after 9 hours, with **2** achieving similar yields with additional time while **3** reached a maximum yield of 17% over 24 hours. A similar trend was observed for **reaction 3**, though the reaction was overall slower and lower yielding for each catalyst, with **1** reaching 84% yield over 24 hours.

Considering the sterically hindered substrates, we observed that **1** was the highest yielding against the di-*ortho*-substituted electrophile (**reaction 4**, 69% after 12 h). When using 2,4,6-trimethylbenzeneboronic acid as the nucleophile (**reaction 5**), **2** was highest yielding

at 12h (94%), while **1** required additional reaction time (78% at 12h; 95% at 24 h). Finally, when employing two heterocyclic coupling partners in **reaction 6**, we observed that **3** was most efficient, reaching nearly quantitative yield after 7 hours. Precatalyst **1** was lowest yielding for this reaction (49%, 24 h).

Overall, we observed that (i) no one precatalyst was uniformly optimal for all substrates and (ii) a precatalyst could be high yielding in one case and low yielding in another (e.g., precatalyst **3** with an 8% yield in **reaction 4** and 99% yield in **reaction 6**). Further, we observed that **2** and **3** exhibited notably different performances in several of the reactions surveyed in spite of their common backbone motif. The lower yields for **3** in **reactions 2** through **5** relative to both **1** and **2** prompted us to consider the role of ligation state in promoting these transformations; in particular, we sought to evaluate the intermediacy and role of  $P_1Ni$  in catalysis. While mechanistic studies of  $P_1M$  species have often focused on monophosphines in Pd SMCs,  $P_1M$  bisphosphine species have previously been proposed for both Pd and Ni-catalyzed processes.<sup>36,37,38</sup> Though our prior work demonstrated that formation of  $P_2Ni$  is essential for successful catalysis, likely to protect the Ni center against off-cycle reactivity and catalyst deactivation, we sought to determine if the transient formation of unsaturated  $P_1Ni$  intermediates plays a role in accelerating the oxidative addition and transmetalation steps of the catalytic cycle. To this end, we utilized **reactions 4** through **6** as case studies, as they highlight cases where each of the three ligands is highest performing.

### Sterically hindered oxidative addition

In **reaction 4**, which features a di-*ortho* substituted aryl chloride, we observed that the bisphosphine catalysts were significantly lower yielding than the monophosphines (*vide supra*).<sup>39</sup> Considering the potential role of ligation state in the oxidative addition step, we sought to monitor the rate of formation of the oxidative adduct of 2-chloro-*meta*-xylene and a  $(CyTyranPhos)_2Ni^0$  species in the presence of increasing equivalents of added ligand. Due to the complicated speciation of  $Ni(COD)_2$  with  $CyTyranPhos$ , we elected to use a  $(CyTyranPhos)_2Ni$ (naphthalene) complex (**4**) synthesized by the reduction of the corresponding  $L_2NiCl_2$  complex with magnesium in the presence of naphthalene.<sup>40,41</sup> High temperature <sup>1</sup>H NMR enabled us to track the formation of  $(CyTyranPhos)_2Ni(xylyl)(Cl)$  (**5**) *in situ* (Figure 4). As shown by the reaction profiles, the rate of oxidative addition is attenuated in the presence of increasing amounts of free ligand. The observed inverse order in ligand indicates that a ligand dissociation event occurs prior to oxidative addition, implicating a  $P_1Ni$  species in catalysis.<sup>42</sup> This observation is consistent with proposed intermediates in Pd-catalyzed  $C(sp^2)-Cl$  oxidative addition, where  $P_1Pd$  is invoked as the active species.<sup>43,44,45</sup>

Having observed this inverse dependence on ligand in oxidative addition, we then computationally probed the relative energetics of mono- and bisligated oxidative addition pathways using density functional theory (DFT) to determine which pathway is more favorable for each of the three ligands surveyed. Oxidative addition transition states for  $P_1Ni$  and  $P_2Ni$  species of each ligand were identified (Figure 5a). Barriers were determined from the  $P_2Ni^0(arene)$  (where arene = 2-chloro-*meta*-xylene) ground state modeled with  $\eta^2$ -arene



coordination. Both transition states were modeled as concerted oxidative addition processes into the C(sp<sup>2</sup>)-Cl bond. Bisphosphine P<sub>1</sub>Ni structures were computed with  $\kappa^1$  binding of the ligand, where the second arm is rotated away from the metal about the ferrocenyl backbone.

Comparing the calculated free energy of activation ( $G^\ddagger$ ) for both the P<sub>2</sub>Ni and P<sub>1</sub>Ni transition states (Figure 5b), we identified that CyTyrannoPhos had a lower barrier for the monoligated pathway, while dcyph and dppf exhibited lower barriers for their bisligated pathways. Interestingly, we also identified that the P<sub>1</sub>Ni<sup>0</sup> ground state species is lower in energy than the corresponding P<sub>2</sub>Ni<sup>0</sup> species for CyTyrannoPhos, while dcyph and dppf were determined to have lower energy P<sub>2</sub>Ni<sup>0</sup> species (Table S25).

Taken together, the experimental and computational results provide some insight into the observed discrepancies in reactivity between the two ligand classes for **reaction 4**. We hypothesize that the increased product yields with the monophosphine precatalyst can be attributed in part to oxidative addition through an energetically accessible P<sub>1</sub>Ni pathway. The lower catalytic yields seen for the bisphosphines imply that oxidative addition along the P<sub>2</sub>Ni pathway is less efficient, allowing for decomposition of the Ni<sup>0</sup> intermediates and comproportionation of Ni<sup>0</sup> with Ni<sup>II</sup> species to generate catalytically inactive Ni<sup>I</sup>.<sup>17</sup> Previous studies of Ni-catalyzed oxidative addition that invoke P<sub>1</sub>Ni pathways involve cleavage of C(sp<sup>2</sup>)-O bonds of phenol derivatives, like carbonates, esters, and sulfamates, that stabilize the unsaturated Ni center through secondary interactions with the substrate leaving group.<sup>46,47,48,49</sup> For example, the Houk group proposed that selective C(sp<sup>2</sup>)-O activation of an aryl ester by a (PCy<sub>3</sub>)Ni catalyst proceeds via a monoligated transition state in which the carbonyl oxygen of the ester is coordinated to Ni.<sup>50</sup> The results presented here, however, also suggest that P<sub>1</sub>Ni species are relevant in oxidative addition processes for which secondary interactions with the electrophile leaving group are not present and contribute to overall catalytic performance of a ligand system. By this analysis, we also anticipated that monophosphines with less-favorable ligand dissociation would be similarly low-yielding with this substrate (*vide infra*). Moreover, for sterically-challenging oxidative additions, labile monophosphine systems would be expected to outperform more rigid bisphosphines.

### Sterically hindered transmetalation

We next shifted our attention to **reaction 5**, in which the nucleophilic coupling partner has di-*ortho* substitution. Here, we observed that **2** was the highest yielding precatalyst at 12 hours; precatalyst **1** was also high yielding, though required additional reaction time to achieve comparable yields. The low yields associated with **3** prompted us to probe the stoichiometry of the catalyst during transmetalation.<sup>51</sup> Using CyTyrannoPhos as our model system, we applied the method of continuous variation (MCV) to **reaction 5** (Figure 6a).<sup>52</sup> Holding the overall mole percent of Ni and ligand constant, the mole fraction ( $\chi$ ), or ratio of ligand to metal, was incrementally varied and the initial rates of product formation were collected at each mole fraction. As shown in Figure 6a, we found that the fastest rate of product formation occurred at  $\chi = 0.5$ , corresponding to 1:1 monophosphine to Ni stoichiometry at the turnover limiting step. Given that the



oxidative addition of this electrophile occurs rapidly at room temperature (see Supporting Information), transmetalation is proposed to be turnover limiting for this substrate pairing and thus the step for which 1:1 Ni:phosphine stoichiometry ( $P_1Ni$ ) is required.<sup>48,53</sup>

These results suggest that ligand dissociation to form an  $P_1Ni$  species is necessary for transmetalation, and thus ligand systems with greater lability will accelerate this step. This finding agrees with stoichiometric transmetalation studies performed by Grimaud and coworkers showing kinetic inhibition for biaryl formation from a  $(PPh_3)_2Ni^{II}$  oxidative adduct and phenylboronic acid in the presence of added  $PPh_3$ .<sup>20</sup> The proposed pre-transmetalation intermediate for both Ni and Pd catalysis exhibits two-point binding of a hydroxyboronate moiety to form a four-coordinate metal center bearing a single phosphine (Figure 6b).<sup>6,7</sup> For bisphosphine ligands, formation of this monoligated intermediate requires dissociation of one ligand arm to form the corresponding  $P_1Ni^{II}$  species. Thus, a bisphosphine with increased lability is expected to be more efficient in the transmetalation step. While **3** evidently can undergo transmetalation, as it is a competent ligand in Ni SMCs, we hypothesize that the inefficiency of transmetalation to this sterically-hindered nucleophile makes the catalyst vulnerable to off-cycle processes, as evidenced by the formation of protodehalogenated substrate (2% fluorobenzene after 12 h).<sup>17</sup>

The kinetic data, in combination with the observed similarities in the reactivity profiles of **1** and **2** (*vide supra*), suggests that dcyph exhibits greater lability in catalysis to enable efficient access to  $P_1Ni^{II}$  intermediates. To probe the role of bisphosphine flexibility in transmetalation, we tested a series of Ni precatalysts bearing 1,2-bis(diphenylphosphino)alkyl ligands with increasing alkyl linker chain lengths in catalysis (Figure 7). Increasing the alkyl linker length increases the conformational flexibility of the ligand and destabilizes the resulting chelate to make dissociation of one arm more favorable, which we hypothesized would enable higher yields. The corresponding  $Ni^{II}(2,4,6\text{-trimethylphenyl})(Br)$  precatalysts (dppe (**6**); dppp (**7**); dppb (**8**), Fig. 7), as well as the corresponding  $Ni(COD)_2$  and ligand catalyst mixtures, were subjected to **reaction 5**.<sup>54</sup> Though these precatalysts were not high yielding for **reaction 5**, we observed that increased linker length resulted in higher yields. In particular, the yield increased significantly between the *cis*-bound **7** to *trans*-bound **8** (3% yield versus 24% yield). Taken together, these experiments suggest that increased backbone flexibility is beneficial for catalysis as it enables the formation of an unsaturated  $P_1Ni$  center that can more efficiently undergo transmetalation.

While our kinetic analysis with  $(CyTyrannoPhos)_nNi$  invokes a  $P_1Ni$  species, precatalyst **2** was found to be the most efficient precatalyst in **reaction 5**. To rationalize this observation, we considered off-cycle reactivity that impacts the overall efficiency of the monophosphine system by looking at side product formation. We observed greater amounts of mesitylene, the product of protodeboronation of the nucleophile, being formed by the monophosphine precatalyst **1** as compared to the reaction using **2** (Table 1). By contrast, protodehalogenation of the electrophile was not observed with **1**, while only trace protodehalogenated electrophile was observed with **2**.

Under common SMC conditions using stoichiometric base and water, base-mediated protodeboronation can occur, particularly for a less-efficient catalyst that is consuming substrate less rapidly and for less stable boronic acids.<sup>55</sup> If base-mediated protodeboronation was the sole mechanism for formation of mesitylene in the reaction, one would expect that, after forming nearly quantitative yields of product after 12 hours, the reaction employing **2** would still incur significant protodeboronation of the remaining ~4 equiv of substrate over the next 24 hours. However, as shown in Table 1, the overall amounts of mesitylene formed in the presence of **2** remain low even after 90% yield is attained at 12 hours. These results suggest that catalyst-mediated protodeboronation occurs, and that its occurrence is a function of ligand. We hypothesize that protodeboronation occurs to a greater extent with **1** due to the formation of a greater amount of coordinatively unsaturated Ni in solution.<sup>56</sup> By contrast, while dcyph can access a P<sub>1</sub>Ni species to generate a highly reactive catalyst, the proximity of the second arm of the phosphine can shield the Ni center from unproductive chemistry.

### Reactivity of monophosphines as a function of steric features

The role of P<sub>1</sub>Ni species identified in the previous two case studies helps to rationalize why precatalyst **1** is high-yielding in **reactions 4** and **5**. However, within monophosphine chemical space, we suspected that ligand steric properties also contribute to the ability to access P<sub>1</sub>Ni species. Indeed, in our HTE study of monophosphines in Ni SMCs, we observed low reactivity for monophosphines with %  $V_{\text{bur}}$  (*min*) values below ~28%. Moreover, computational analysis of the  $\Delta G$  of phosphine dissociation for monophosphine P<sub>2</sub>Ni(benzaldehyde) complexes indicated that ligand dissociation becomes increasingly favorable with increasing values of %  $V_{\text{bur}}$  (*min*).<sup>13</sup>

This prompted us to consider how monophosphine steric features impact reactivity in **reactions 4** and **5**, given the need to form unsaturated P<sub>1</sub>Ni species in catalysis. For this comparison, we utilized a series of four monophosphine precatalysts, including **1**, that share a common mixed alkyl-aryl scaffold but vary in the magnitude of both their calculated %  $V_{\text{bur}}$  (*min*) and cone angle features. Both MePPh<sub>2</sub> (precatalyst **9**) and CyPPh<sub>2</sub> (precatalyst **10**) have unsubstituted aryl groups, while MeTyranPhos (methyl(3,5-di-*tert*-butylphenyl)phosphine) (precatalyst **11**) and CyTyranPhos (precatalyst **1**) include bulky *t*-Bu groups that increase their measured cone angles (Figure 8). Within each pairing in this series, we observed lower yields for the precatalyst with a smaller %  $V_{\text{bur}}$  (*min*). Overall, however, both ligands possessing greater steric bulk, as quantified by their larger cone angles, were higher yielding across the three reactions surveyed, with precatalyst **1** the highest yielding in the series.

Given the proposed role of P<sub>1</sub>Ni species in catalysis, we hypothesize that the improved performance of **1** over similar monophosphine-ligated precatalysts can, in part, be attributed to its steric profile that enables more facile formation of unsaturated intermediates in catalysis. The higher %  $V_{\text{bur}}$  (*min*) of CyTyranPhos (27.7%) as compared to MeTyranPhos (25.3%), for example, captures its ability to dissociate from P<sub>2</sub>Ni species more readily in catalysis. Indeed, when we combine a mixture of **1** with 2 equivalents of MeTyranPhos, we see full conversion of **1** in 12 hours to form both the mixed

ligand species and **11** (Figure 8b). By contrast, the reverse process occurs very slowly, only partially converting complex **11** to the corresponding mixed complex, suggesting that dissociation of the lower %  $V_{\text{bur}}$  (*min*) phosphine is less thermodynamically and kinetically favorable.

To gain insight into the mechanism of ligand dissociation from **1**, we performed  $^{31}\text{P}$  2D EXSY experiments with increasing equivalents of added CyTyranPhos. Analysis of degenerate ligand exchange between **1** and free CyTyranPhos (1.0, 5.0, and 10.0 equivalents) revealed that the rate of ligand exchange does not change with increasing concentration of free ligand (Figure 9, see Figures S20–S22). This supports a dissociative mechanism of ligand exchange, consistent with the hypothesis that **1** is substitutionally labile and enables formation of  $\text{P}_1\text{Ni}$  intermediates during catalysis.<sup>57</sup>

Additionally, the higher yields seen for **11** and **1** as compared to their undecorated analogues (**9** and **10**, respectively) indicate that the remote steric bulk described by cone angle is beneficial for catalysis, potentially through mediating ligand dissociation dynamics or stabilizing catalytic intermediates. Overall, these observations reinforce that %  $V_{\text{bur}}$  (*min*) is the dominant feature controlling ligation state and the favorability of ligand dissociation.

### Reactivity of heteroaryl substrates

Though dppf-ligated precatalyst **3** was lower yielding for **reactions 1** through **5**, we identified it to be the top performer in **reaction 6** (3-chloropyridine with 2-thienylboronic acid), reaching 95% yield in 7 hours. By contrast, this was the lowest yielding reaction for **1** (40% at 7h; 49% over 24 h). The use of heteroaromatic coupling partners in Ni catalysis can be challenging owing to the ability of these substrates to bind to and poison the catalyst. Further, while Ni-catalyzed SMCs commonly require elevated temperatures and stoichiometric water and base, heteroaromatic boronic acids are susceptible to protodeboronation under these conditions.<sup>58</sup> Hartwig and coworkers demonstrated that a (dppf)Ni(cinnamyl)(Cl) precatalyst enabled the synthesis of several hetero-biaryl compounds under relatively mild conditions (0.5 mol% catalyst loading at 50 °C).<sup>59</sup> Given this precedent, the observed high yields with **3** in **reaction 6** were unsurprising and prompted further investigation into the origin of the increased activity of the bisphosphine precatalysts relative to the monophosphine precatalyst.

We first identified whether one or both coupling partners were low-yielding with CyTyranPhos-ligated precatalyst **1** by cross-coupling each with a non-heteroaromatic substrate. Using 3-chloropyridine as the electrophile (**reaction 7**, Scheme 2), all three precatalysts achieved near quantitative yields. By contrast, we found that the **1** was low-yielding in the reaction of 2-thiophenylboronic acid with 1-chloro-4-fluorobenzene (**reaction 8**, Figure 10, entry 1), while both **2** and **3** again achieved high yields (Table S14). Considering the possibility of protodeboronation liberating free thiophene in the reaction mixture, we tested catalysis in the presence of 1 and 2 equivalents of added thiophene (Figure 10, entries 2 and 3), which resulted in decreased yields. Increasing the equivalents of boronic acid to 5 equivalents (Figure 10, entry 4) further attenuated the reaction yield. In fact, we identified that the highest yields for precatalyst **1** were observed when the boronic

acid loading was lowered to 1.0 equivalent (Figure 10, entry 5). Lastly, we considered the possibility of the product acting as a catalyst poison by adding one equivalent of 2-phenylthiophene (entry 6), which showed no impact on product yield. By contrast, the bisphosphine precatalysts were unaffected by these additives in **reaction 8** (Table S14).

These results suggest that the formation of thiophene by substrate protodeboronation is detrimental to catalysis for the monophosphine system. Attempts to directly observe and quantify the formation of thiophene were unsuccessful due to the instability of the boronic acid. While the protodeboronation data from **reaction 5** suggests that a catalyst-dependent process contributes to thiophene formation, we are unable to distinguish this pathway from the known base-catalyzed protodeboronation of this substrate.<sup>27, 58</sup> Possible mechanisms for catalyst deactivation with thiophene include catalyst trapping by association of the thiophene  $\pi$ -system to a Ni(0) species and oxidative insertion of the Ni catalyst into the C–S bond.<sup>60,61</sup> We hypothesize that the increased lability of the monophosphine-ligated complex results in an increased concentration of P<sub>1</sub>Ni species that are susceptible to deactivation pathways, while the bisphosphine systems remain at P<sub>2</sub>Ni sufficiently to protect the catalyst. Nonetheless, we have observed cases (e.g. **reaction 2**) where all three precatalysts are lower yielding in the presence of a thiophene additive (Table S16), suggesting that overall catalytic efficiency influences how susceptible a given catalyst is to deactivation.

Given the synthetic importance of heterocyclic motifs, we sought to determine if **1** is more broadly incompatible with thiophene-containing substrates by surveying a series of related examples (Figure 11). We found that 2-chlorothiophene (**reaction 9**) was successfully cross-coupled in 90% yield, achieving the identical product to **reaction 8** with the opposite coupling partners. Interestingly, both **2** and **3** were low yielding in this instance (Table S17). Similarly, the 3-thiophenyl boronic acid substrate was cross-coupled successfully (**reaction 10**, 80% yield), in part owing to the increased stability of this substrate as compared to the 2-substituted boronic acid. Cross-coupling with the corresponding 2-furanylboronic acid substrate was also high-yielding with **1** (**reaction 11**), reaching 98% yield when coupled with 1-chloro-4-fluorobenzene and exceeding the yields attained by both **2** and **3** (Table S18). Notably, each of these substrates is less susceptible to byproduct formation relative to 2-thiophenylboronic acid, enabling successful catalysis with the more labile monophosphine system.<sup>58</sup> These studies highlight the additional considerations necessary for catalysis with substrates that can generate a catalyst poison, wherein the overall lability of the complex must be accounted for relative to potential catalyst deactivation pathways.

## CONCLUSION

We have compared the catalytic performance of mono- and bisphosphine Ni precatalysts in SMCs of diverse substrate pairings. Catalytic, kinetic, and computational data demonstrate that P<sub>1</sub>Ni species are responsible for enabling challenging oxidative addition and transmetalation steps, while P<sub>2</sub>Ni species help to prevent off-cycle reactivity and catalyst poisoning. For reactions involving electronically deactivated or sterically hindered substrates, the use of a monophosphine like CyTyrannoPhos is advantageous for generating highly reactive P<sub>1</sub>Ni intermediates. To enable ligand dissociation, monophosphines should have a %  $V_{bur}$  (*min*) that approaches but does not exceed the ligation state threshold (~32%).

In reactions employing substrates that are subject to protodefunctionalization or can serve as a catalyst poison, bisphosphines provide a synthetic advantage by preferentially forming chelated  $P_2Ni$  species.<sup>62</sup> Use of a wider bite angle bisphosphine, like dcyph, can furnish a more active catalyst against electronically or sterically challenging substrates.

These findings are summarized in Figure 12 to establish guidelines for selecting a ligand class in a range of synthetic applications. Additional considerations regarding the electronic and steric properties of a given ligand contribute to its overall effectiveness and should be included in ligand design and selection. As defined by our study, the ideal phosphine ligand for Ni-catalyzed SMCs and related reactions proceeding through similar organometallic intermediates must balance the ability to form both mono- and bisligated intermediates during catalysis. Ultimately, this study provides guidance for ligand selection as a function of substrate properties and informs the development of new ligands for Ni-catalyzed SMCs.

## Supplementary Material

Refer to Web version on PubMed Central for supplementary material.

## ACKNOWLEDGMENTS

We thank Dr. István Pelczer and Ken Conover for assistance with high-temperature and EXSY NMR experiments and Dr. Phil Jeffrey for X-ray crystallographic characterization. Financial support for this work was provided by the NIGMS (R35 GM126986).

### Funding Sources

NIGMS (R35 GM126986)

## REFERENCES

- (1). Johansson Seechurn CCC; Kitching MO; Colacot TJ; Snieckus V Palladium-Catalyzed Cross-Coupling: A Historical Contextual Perspective to the 2010 Nobel Prize. *Angew. Chem. Int. Ed* 2012, 51, 5062–5085.
- (2). Hazari N; Melvin PR; Beromi MM Well-defined nickel and palladium precatalysts for cross-coupling. *Nat. Rev. Chem* 2017, 1, 0025. [PubMed: 29034333]
- (3). Campeau L-C; Hazari N Cross-Coupling and Related Reactions: Connecting Past Success to the Development of New Reactions for the Future. *Organometallics* 2019, 38, 3–35. [PubMed: 31741548]
- (4). Lavoie CM; Stradiotto M Bisphosphines: A Prominent Ancillary Ligand Class for Application in Nickel-Catalyzed C–N Cross-Coupling. *ACS Catal.* 2018, 8, 7228–7250.
- (5). Hartwig JF; Paul F Oxidative Addition of Aryl Bromide after Dissociation of Phosphine from a Two-Coordinate Palladium(0) Complex, Bis(tri-*o*-tolylphosphine)Palladium(0). *J. Am. Chem. Soc* 1995, 117, 5373–5374.
- (6). Thomas AA; Denmark SE Pre-transmetalation intermediates in the Suzuki-Miyaura reaction revealed: The missing link. *Science* 2016, 352, 329–332. [PubMed: 27081068]
- (7). Thomas AA; Wang H; Zahrt AF; Denmark SE Structural, Kinetic, and Computational Characterization of the Elusive Arylpalladium(II)boronate Complexes in the Suzuki–Miyaura Reaction. *J. Am. Chem. Soc* 2017, 139, 3805–3821. [PubMed: 28266847]
- (8). Firsan SJ; Sivakumar V; Colacot TJ Emerging Trends in Cross-Coupling: Twelve-Electron-Based  $L_1Pd(0)$  Catalysts, Their Mechanism of Action, and Selected Applications. *Chem. Rev* 2022, 122, 16983–17027. [PubMed: 36190916]

- (9). Martin R; Buchwald SL Palladium-catalyzed Suzuki-Miyaura cross-coupling reactions employing dialkylbiaryl phosphine ligands. *Acc. Chem. Res* 2008, 41, 1461–1473. [PubMed: 18620434]
- (10). Fu GC The development of versatile methods for palladium-catalyzed coupling reactions of aryl electrophiles through the use of P(t-Bu)<sub>3</sub> and PCy<sub>3</sub> as ligands. *Acc. Chem. Res* 2008, 41, 1555–1564. [PubMed: 18947239]
- (11). Chen L; Ren P; Carrow BP Tri(1-adamantyl)phosphine: Expanding the Boundary of Electron-Releasing Character Available to Organophosphorus Compounds. *J. Am. Chem. Soc* 2016, 138, 6392–6395. [PubMed: 27164163]
- (12). Wu K; Doyle AG Parameterization of phosphine ligands demonstrates enhancement of nickel catalysis via remote steric effects. *Nat. Chem* 2017, 9, 779–784. [PubMed: 28754948]
- (13). Newman-Stonebraker SH; Smith SR; Borowski JE; Peters E; Gensch T; Johnson HC; Sigman MS; Doyle AG Univariate classification of phosphine ligation state and reactivity in cross-coupling catalysis. *Science* 2021, 374, 301–308. [PubMed: 34648340]
- (14). Newman-Stonebraker SH; Wang JY; Jeffrey PD; Doyle AG Structure–Reactivity Relationships of Buchwald-Type Phosphines in Nickel-Catalyzed Cross-Couplings. *J. Am. Chem. Soc* 2022, 144, 19635–19648. [PubMed: 36250758]
- (15). N-heterocyclic carbene ligands (NHCs) have also been successfully implemented as ancillary ligands in SMCs using Pd and Ni. We have limited the scope of our study to phosphine ligands. See Ref. 2 and the following references for information about the application of this ligand class. (a) Marion N; Nolan SP Well-Defined N-Heterocyclic Carbenes–Palladium(II) Precatalysts for Cross-Coupling Reactions. *Acc. Chem. Res* 2008, 41, 1440–1449 [PubMed: 18774825] (b) Diez-González S; Marion N; Nolan SP N-Heterocyclic Carbenes in Late Transition Metal Catalysis. *Chem. Rev* 2009, 109, 3612–3676 [PubMed: 19588961]
- (16). Standley EA; Smith SJ; Müller P; Jamison TF A Broadly Applicable Strategy for Entry into Homogeneous Nickel(0) Catalysts from Air-Stable Nickel(II) Complexes. *Organometallics* 2014, 33, 2012–2018. [PubMed: 24803717]
- (17). Mohadjer Beromi M; Nova A; Balcells D; Brasacchio AM; Brudvig GW; Guard LM; Hazari N; Vinyard DJ Mechanistic Study of an Improved Ni Precatalyst for Suzuki–Miyaura Reactions of Aryl Sulfamates: Understanding the Role of Ni(I) Species. *J. Am. Chem. Soc* 2017, 139, 922–936. [PubMed: 28009513]
- (18). Ge S; Hartwig JF Highly Reactive, Single-Component Nickel Catalyst Precursor for Suzuki–Miyaura Cross-Coupling of Heteroaryl Boronic Acids with Heteroaryl Halides. *Angew. Chem. Int. Ed* 2012, 51, 12837–12841.
- (19). Mohadjer Beromi M; Banerjee G; Brudvig GW; Charboneau DJ; Hazari N; Lant HMC; Mercado BQ Modifications to the Aryl Group of dppf-Ligated Ni  $\sigma$ -Aryl Precatalysts: Impact on Speciation and Catalytic Activity in Suzuki–Miyaura Coupling Reactions. *Organometallics* 2018, 37, 3943–3955. [PubMed: 31736532]
- (20). Payard P-A; Perego LA; Ciofini I; Grimaud L Taming Nickel-Catalyzed Suzuki-Miyaura Coupling: A Mechanistic Focus on Boron-to-Nickel Transmetalation. *ACS Catal.* 2018, 8, 4812–4823.
- (21). Ariki ZT; Maekawa Y; Nambo M; Crudden CM Preparation of Quaternary Centers via Nickel-Catalyzed Suzuki–Miyaura Cross-Coupling of Tertiary Sulfones. *J. Am. Chem. Soc* 2018, 140, 78–81. [PubMed: 29215881]
- (22). Gensch T; dos Passos Gomes G; Friederich P; Peters E; Gaudin T; Pollice R; Jorner K; Nigam A; Lindner-D'Addario M; Sigman MS; Aspuru-Guzik A A Comprehensive Discovery Platform for Organophosphorus Ligands for Catalysis. *J. Am. Chem. Soc* 2022, 144, 1205–1217. [PubMed: 35020383]
- (23). Quasdorf KW; Riener M; Petrova KV; Garg NK Suzuki–Miyaura Coupling of Aryl Carbamates, Carbonates, and Sulfamates. *J. Am. Chem. Soc* 2009, 131, 17748–17749. [PubMed: 19928764]
- (24). Ramgren SD; Hie L; Ye Y; Garg NK Nickel-Catalyzed Suzuki–Miyaura Couplings in Green Solvents. *Org. Lett* 2013, 15, 3950–3953. [PubMed: 23879392]
- (25). Malineni J; Jezorek RL; Zhang N; Percec V An Indefinitely Air-Stable  $\sigma$ -Ni<sup>II</sup> Precatalyst for Quantitative Cross-Coupling of Unreactive Aryl Halides and Mesylates with Aryl Neopentylglycolboronates. *Synthesis* 2016, 48, 2795–2807.



- (26). Hansch C; Leo A; Taft RW A survey of Hammett substituent constants and resonance and field parameters. *Chem. Rev* 1991, 91, 165–195.
- (27). West MJ; Watson AJB Ni vs. Pd in Suzuki–Miyaura  $sp^2$ – $sp^2$  cross-coupling: a head-to-head study in a comparable precatalyst/ligand system. *Org. Biomol. Chem* 2019, 17, 5055–5059. [PubMed: 31049539]
- (28). Bajo S; Laidlaw G; Kennedy AR; Sproules S; Nelson DJ Oxidative Addition of Aryl Electrophiles to a Prototypical Nickel(0) Complex: Mechanism and Structure/Reactivity Relationships. *Organometallics* 2017, 36, 1662–1672.
- (29). While DPEPhos was also high yielding in both reactions, we were unable to access the (DPEPhos)Ni( $\alpha$ -tolyl)(Cl) precatalyst.
- (30). Barth EL; Davis RM; Mohadjer Beromi M; Walden AG; Balcells D; Brudvig GW; Dardir AH; Hazari N; Lant HMC; Mercado BQ; Peczak IL Bis(dialkylphosphino)ferrocene-Ligated Nickel(II) Precatalysts for Suzuki–Miyaura Reactions of Aryl Carbonates. *Organometallics* 2019, 38, 3377–3387. [PubMed: 32565607]
- (31). Kuwano R; Shimizu R An Improvement of Nickel Catalyst for Cross-coupling Reaction of Arylboronic Acids with Aryl Carbonates by Using a Ferrocenyl Bisphosphine Ligand. *Chem. Lett* 2011, 40, 913–915.
- (32). Guard LM; Mohadjer Beromi M; Brudvig GW; Hazari N; Vinyard DJ Comparison of dppf-Supported Nickel Precatalysts for the Suzuki–Miyaura Reaction: The Observation and Activity of Nickel(I). *Angew. Chem. Int. Ed* 2015, 54, 13352–13356
- (33). Shields JD; Gray EE; Doyle AG A Modular, Air-Stable Nickel Precatalyst. *Org. Lett* 2015, 17, 2166–2169. [PubMed: 25886092]
- (34). These values were determined from X-ray crystallographic data of complexes **2** and **3** from reference 16 using SambVca 2.1.23
- (35). Falivene L; Cao Z; Petta A; Serra L; Poater A; Oliva R; Scarano V; Cavallo L Towards the online computer-aided design of catalytic pockets. *Nat. Chem* 2019, 11, 872–879. [PubMed: 31477851]
- (36). Portnoy M; Milstein D Mechanism of aryl chloride oxidative addition to chelated palladium(0) complexes. *Organometallics* 1993, 12, 1665–1673.
- (37). Payard P-A; Bohn A; Tocqueville D; Jaouadi K; Escoude E; Ajig S; Dethoor A; Gontard G; Perego LA; Vitale M; Ciofini I; Wagschal S; Grimaud L Role of dppf Monoxide in the Transmetalation Step of the Suzuki–Miyaura Coupling Reaction. *Organometallics* 2021, 40, 1120–1128.
- (38). Indolese AF Suzuki-type coupling of chloroarenes with arylboronic acids catalysed by nickel complexes. *Tet. Lett* 1997, 38, 3513–3516.
- (39). Sterically-hindered substrates have been shown to be effective with **3** when employing aryl sulfamate electrophiles. See reference 17 for details.**3**
- (40). Scott F; Krüger C; Betz P Preparation of new nickel(0) naphthalene complexes, crystal structure of [Ni(C<sub>10</sub>H<sub>8</sub>)(i-C<sub>3</sub>H<sub>7</sub>)<sub>2</sub>PCH<sub>2</sub>CH<sub>2</sub>P(*i*-C<sub>3</sub>H<sub>7</sub>)<sub>2</sub>]. *J. Organomet. Chem* 1990, 387, 113–121.
- (41). Stanger A; Shazar A A one-pot method for the preparation of (R<sub>3</sub>P)<sub>2</sub>Ni<sup>0</sup>L complexes. *J. Organomet. Chem* 1993, 458, 233–236.
- (42). Another potential rationale for the observation of an inverse order in ligand would involve ligand dissociation from an L<sub>3</sub>Ni species. While this species can be formed with smaller monophosphines, we have not observed significant formation of this species with CyTyranPhos. See Figure S12 for spectroscopic data.<sup>3</sup>
- (43). Barrios-Landeros F; Carrow BP; Hartwig JF Effect of ligand steric properties and halide identity on the mechanism for oxidative addition of haloarenes to trialkylphosphine Pd(0) complexes. *J. Am. Chem. Soc* 2009, 131, 8141–8154. [PubMed: 19469511]
- (44). Li Z; Fu Y; Guo Q-X; Liu L Theoretical Study on Monoligated Pd-Catalyzed Cross-Coupling Reactions of Aryl Chlorides and Bromides. *Organometallics* 2008, 27, 4043–4049.
- (45). Schoenebeck F; Houk KN Ligand-controlled regioselectivity in palladium-catalyzed cross coupling reactions. *J. Am. Chem. Soc* 2010, 132, 2496–2497. [PubMed: 20121156]
- (46). Hooker LV; Neufeldt SR Ligation state of nickel during C–O bond activation with monodentate phosphines. *Tetrahedron* 2018, 74, 6717–6725. [PubMed: 31105349]



- (47). Entz ED; Russell JEA; Hooker LV; Neufeldt SR Small Phosphine Ligands Enable Selective Oxidative Addition of Ar–O over Ar–Cl Bonds at Nickel(0). *J. Am. Chem. Soc* 2020, 142, 15454–15463. [PubMed: 32805116]
- (48). Quasdorf KW; Antoft-Finch A; Liu P; Silberstein AL; Komaromi A; Blackburn T; Ramgren SD; Houk KN; Snieckus V; Garg NK Suzuki–Miyaura Cross-Coupling of Aryl Carbamates and Sulfamates: Experimental and Computational Studies. *J. Am. Chem. Soc* 2011, 133, 6352–6363. [PubMed: 21456551]
- (49). Zhang S-Q; Taylor BLH; Ji C-L; Gao Y; Harris MR; Hanna LE; Jarvo ER; Houk KN; Hong X Mechanism and Origins of Ligand-Controlled Stereoselectivity of Ni-Catalyzed Suzuki–Miyaura Coupling with Benzylic Esters: A Computational Study. *J. Am. Chem. Soc* 2017, 139, 12994–13005. [PubMed: 28838241]
- (50). Hong X; Liang Y; Houk KN Mechanisms and Origins of Switchable Chemoselectivity of Ni-Catalyzed C(aryl)–O and C(acyl)–O Activation of Aryl Esters with Phosphine Ligands. *J. Am. Chem. Soc* 2014, 136, 2017–2025. [PubMed: 24428154]
- (51). We did observe higher yields for precatalyst **3** when cross-coupling 2,4,6-trimethylphenylboronic acid with 4-chloroanisole, though it was still significantly lower yielding than **1** and **2**. See Table S6 for additional data and analysis.**12**
- (52). Renny JS; Tomasevich LL; Tallmadge EH; Collum DB Method of Continuous Variations: Applications of Job Plots to the Study of Molecular Associations in Organometallic Chemistry. *Angew. Chem. Int. Ed* 2013, 52, 11998–12013.
- (53). Li Z; Zhang S-L; Fu Y; Guo Q-X; Liu L Mechanism of Ni-Catalyzed Selective C–O Bond Activation in Cross-Coupling of Aryl Esters. *J. Am. Chem. Soc* 2009, 131, 8815–8823. [PubMed: 19505075]
- (54). Mesityl bromide precatalysts were used in this experiment due to the challenges associated with synthesis and stability of the dppp and dppb Ni<sup>II</sup>(*o*-tolyl)(Cl) precatalysts, as described in reference 16. The increased steric hindrance of the precatalyst likely slows down the rate of precatalyst activation via transmetalation, so the analogous Ni(COD)<sub>2</sub> and ligand systems were also tested.**11**
- (55). Cox PA; Reid M; Leach AG; Campbell AD; King EJ; Lloyd-Jones GC Base-Catalyzed Aryl-B(OH)<sub>2</sub> Protodeboronation Revisited: From Concerted Proton Transfer to Liberation of a Transient Aryl Anion. *J. Am. Chem. Soc* 2017, 139, 13156–13165. [PubMed: 28823150]
- (56). Kuivila HG; Reuwer JF; Mangravite JA Electrophilic Displacement Reactions. XVI. Metal Ion Catalysis in the Protodeboronation of Areneboronic Acids 1–3. *J. Am. Chem. Soc* 1964, 86, 2666–2670.
- (57). The proposed dissociative mechanism of ligand exchange for **1** deviates from the commonly proposed associative mechanism of ligand exchange for 16 electron, d8 square planar complexes (see Hartwig, J. F. *Organotransition Metal Chemistry: From Bonding to Catalysis*; Univ. Science Books, 2010). Study of the ligation state dynamics of CyTyrannoPhos and related ligands are under further investigation in our lab.**1**
- (58). Cox PA; Leach AG; Campbell AD; Lloyd-Jones GC Protodeboronation of Heteroaromatic, Vinyl, and Cyclopropyl Boronic Acids: pH–Rate Profiles, Autocatalysis, and Disproportionation. *J. Am. Chem. Soc* 2016, 138, 9145–9157. [PubMed: 27355973]
- (59). Ge S; Hartwig JF Highly Reactive, Single-Component Nickel Catalyst Precursor for Suzuki–Miyaura Cross-Coupling of Heteroaryl Boronic Acids with Heteroaryl Halides. *Angew. Chem. Int. Ed* 2012, 51, 12837–12841.
- (60). Hannigan MD; Tami JL; Zimmerman PM; McNeil AJ Rethinking Catalyst Trapping in Ni-Catalyzed Thieno[3,2-*b*]thiophene Polymerization. *Macromolecules* 2022, 55, 10821–10830. [PubMed: 37396500]
- (61). He W; Patrick BO; Kennepohl P Identifying the missing link in catalyst transfer polymerization. *Nat. Commun* 2018, 9, 3866. [PubMed: 30250037]
- (62). The role of Ni(I) was not explicitly explored as a function of ligation state and phosphine identity in this study. Given the demonstration of Ni(I) as an off-cycle species by Hazari and coworkers (see reference 17), we imagine that the formation of these species in catalysis through comproportionation would be affected by the ligation state of the catalyst and may account, in part, for some of the differences in catalytic efficiency we observed. In addition, our group has

also recently observed monophosphine Ni(I) intermediates resulting from aryl chloride oxidative addition to Ni(0) species bearing Buchwald-type dialkyl biaryl phosphines (see reference 14). Study of these intermediates is beyond the scope of our current study, but is under further investigation in our lab.

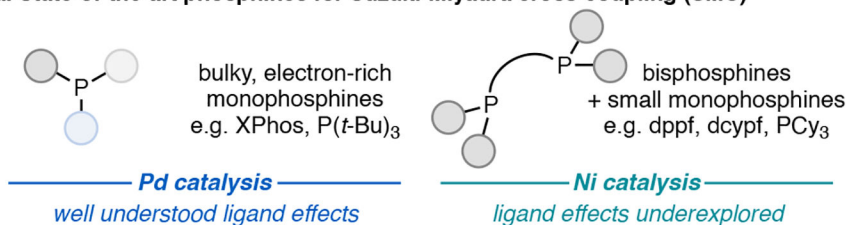
Author Manuscript

Author Manuscript

Author Manuscript

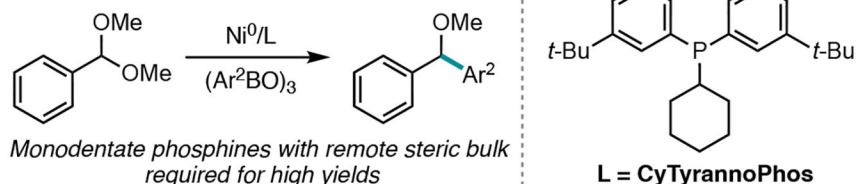
Author Manuscript

**a. State-of-the-art phosphines for Suzuki-Miyaura cross-coupling (SMC)**

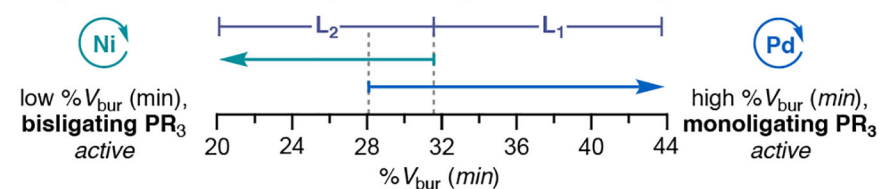


**b. Monophosphines developed for Ni-catalysis**

Doyle 2017:



**c. Ligation state in Ni SMCs: L<sub>2</sub>Ni necessary for reactive catalysts**



**d. This work: comparison of mono v. bisphosphine reactivity in Ni SMCs**

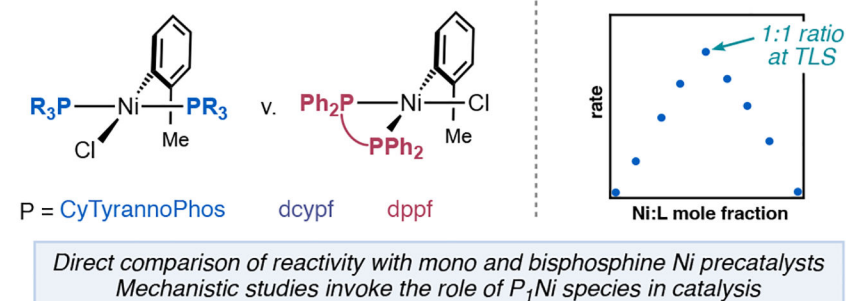
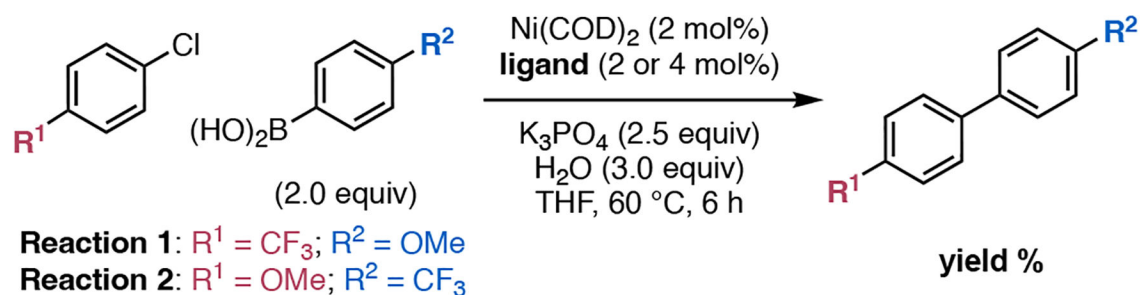


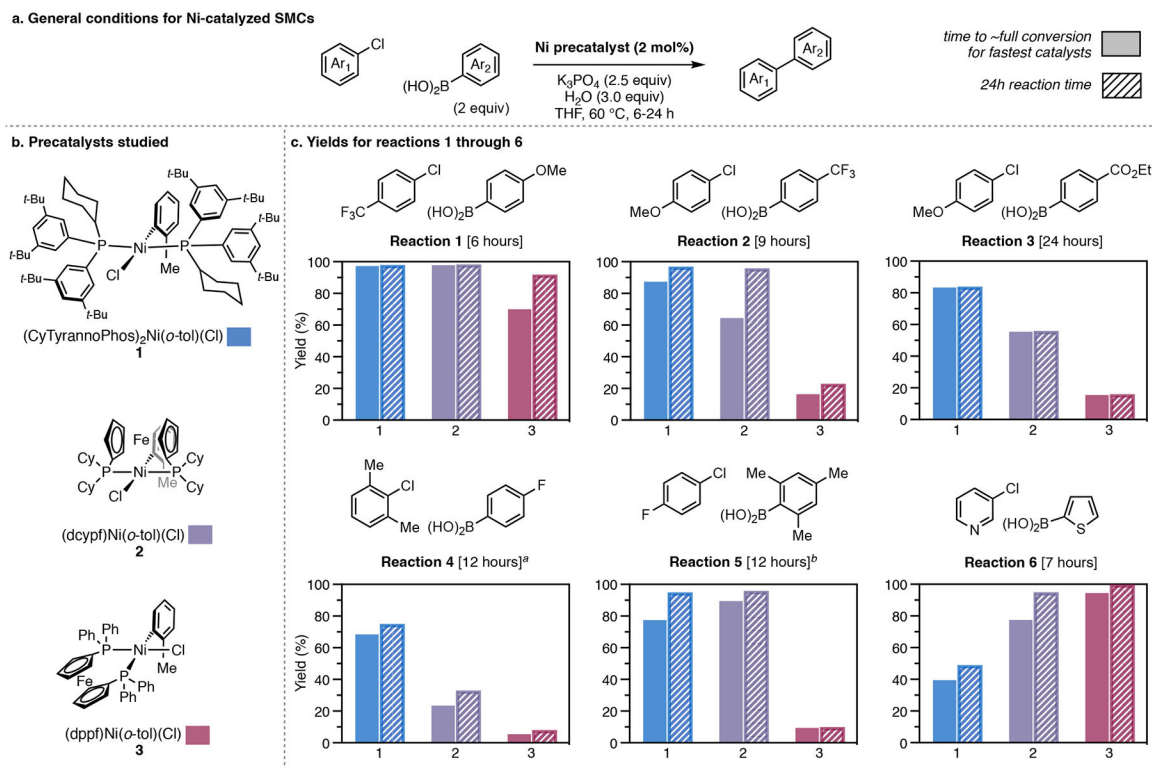
**Figure 1.** Phosphine ligands effects in Ni and Pd-catalyzed Suzuki-Miyaura cross-coupling (SMC). b. Monophosphines for Ni-SMCs. c. Role of catalyst ligation state. d. This work.



	entry	ligand	yield, Rxn 1 (%)	yield, Rxn 2 (%)
monophosphines (4 mol%)	1	PCy <sub>3</sub>	84	61
	2	MePPh <sub>2</sub>	60	22
	3	CyPPh <sub>2</sub>	61	63
	4	CyTyrannoPhos	99	99
	5	CyJohnPhos	97	23
bisphosphines (2 mol%)	6	dppf	64	10
	7	dcypf	74	24
	8	dppe	25	0
	9	dpbz	2	0
	10	DPEPhos	83	16

**Figure 2.**

Initial mono- and bisphosphine ligand screen. Yields determined by GC analysis against a dodecane internal standard and are the average of two experimental runs. Reactions run at 0.05 mmol scale (1 mL THF). See Supporting Information for reaction procedures.

**Figure 3.**

Comparison of precatalyst reactivity in Ni-catalyzed SMCs. **a.** General scheme for catalytic reactions studied. Reactions run at 0.05 mmol scale (1 mL THF). See Supporting Information for reaction procedures. **b.** Ni precatalysts used for comparison study. **c.** Substrate pairings used in Ni-catalyzed SMCs. The time of the first timepoint is shown next to each reaction label. Each plot shows the yields for each of the three precatalysts at the first time point (solid bar) and 24 h (dashed bar). Reactions **1-3** and **6** were analyzed by GC against a dodecane internal standard. Reactions **4** and **5** were analyzed by  $^{19}\text{F}$  NMR against a 1-fluoronaphthalene external standard. <sup>a</sup>Run with 4 mol% Ni and 5 equivalents boronic acid. <sup>b</sup>Run at 80 °C in 1,4-dioxane.

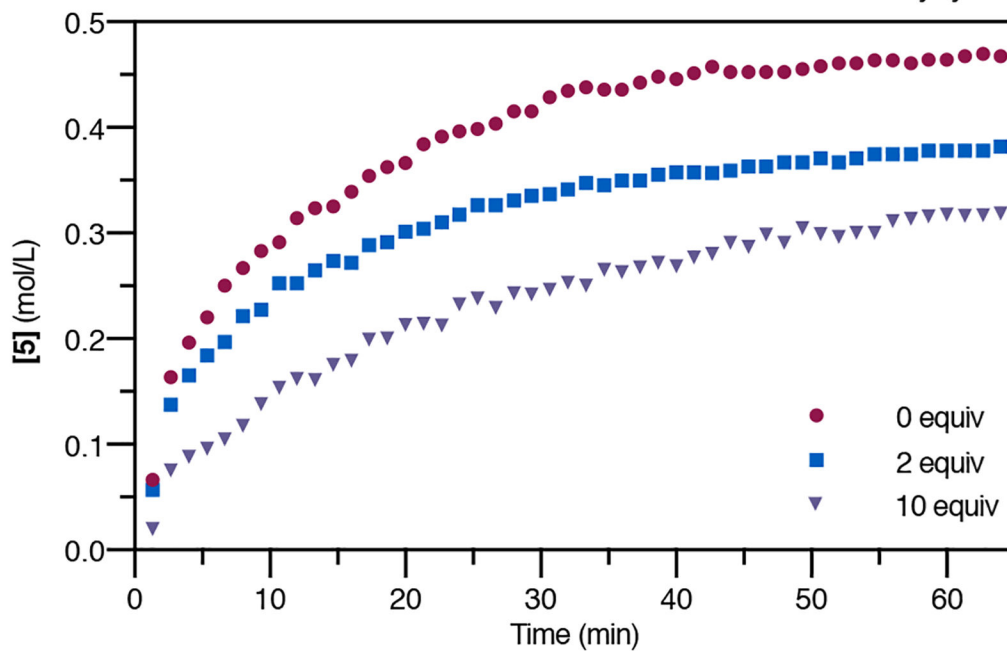
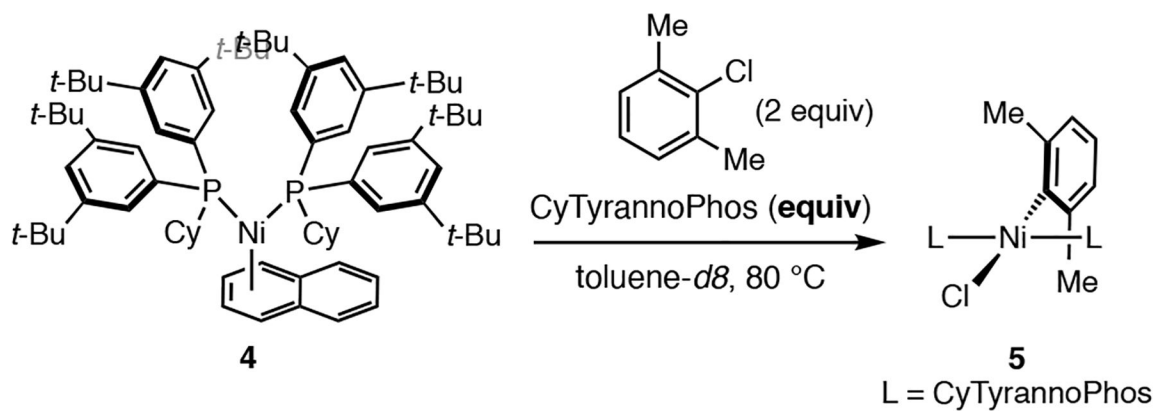
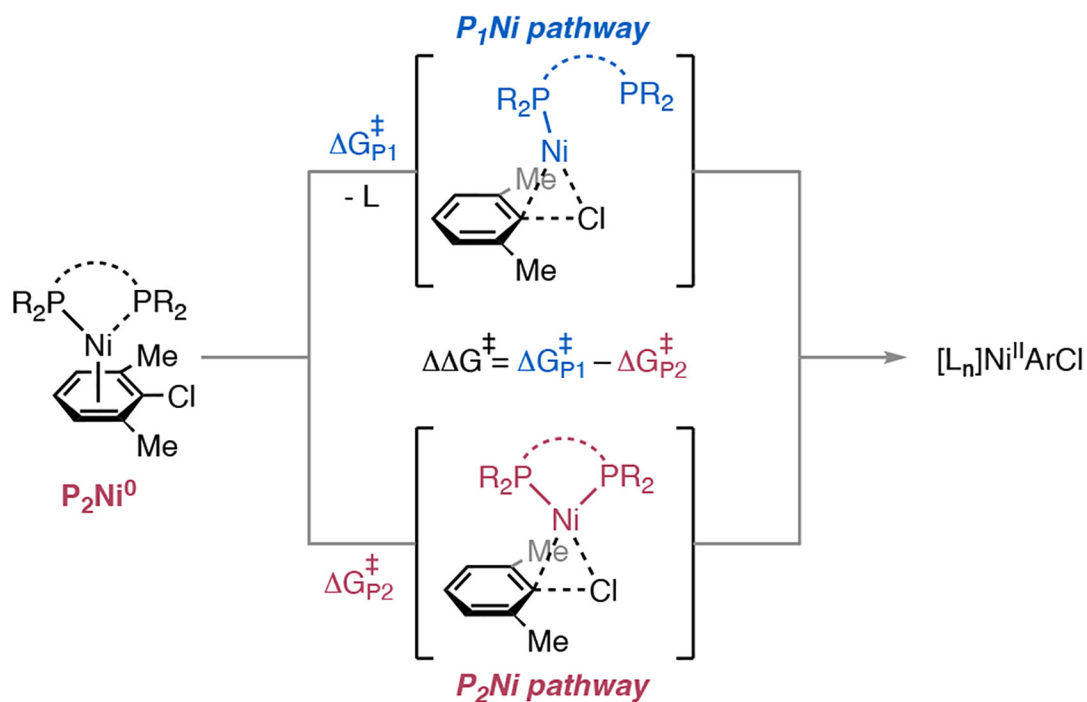


**Figure 4.** Oxidative addition of 2-chloro-*meta*-xylene to **4** in the presence of added equivalents of ligand. Formation of **5** was monitored by  $^1\text{H}$  NMR. See Supporting Information for synthesis of **4** and experimental details.

### a. Schematic of mono and bisligated structures studied by DFT



### b. Relative energetics of mono and bisligated oxidative addition pathways

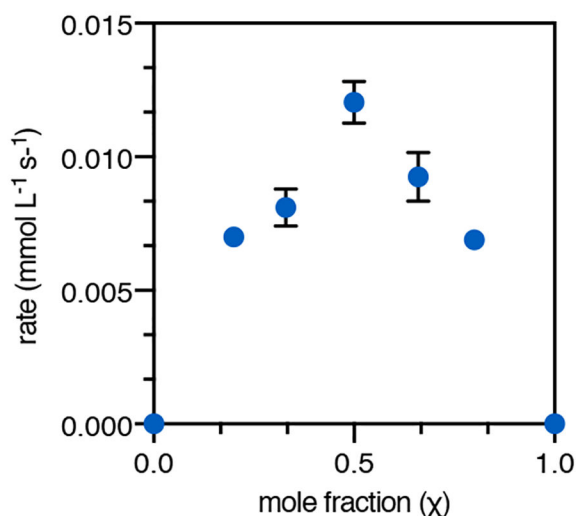
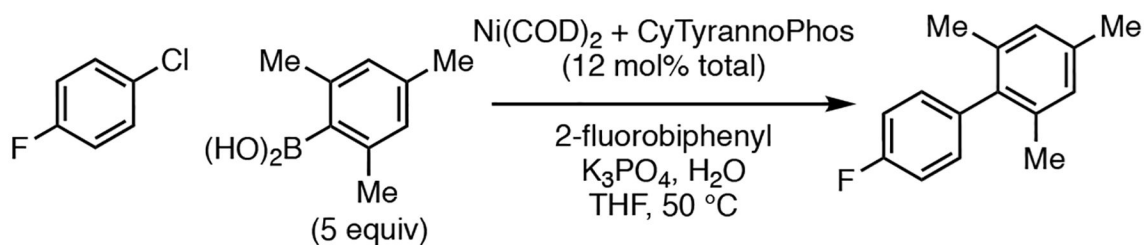
Ligand	$\Delta\Delta G^\ddagger$ (kcal/mol) M06/def-2TZVP	Preferred pathway
CyTyranPhos	-6.0	$P_1$
dcypf	4.0	$P_2$
dppf	8.3	$P_2$

**Figure 5.**

Computational analysis of  $P_1Ni$  and  $P_2Ni$  oxidative addition pathways. **a.** Schematic of two pathways explored. The  $P_1Ni$  pathway for the monophosphine was calculated with one equivalent of free ligand. The  $P_1Ni$  pathway for the bisphosphines are represented with  $\kappa^1$  binding of the ligand, where the curved dotted line represents the ferrocene backbone. **b.** Preferred oxidative addition pathway for each ligand. The free energies of activation were determined by DFT methods at the M06/def2-TZVP/B3LYP-D3/6-31G(d,p) [SDD for Ni and Fe] level of theory with a SMD solvation model (THF).

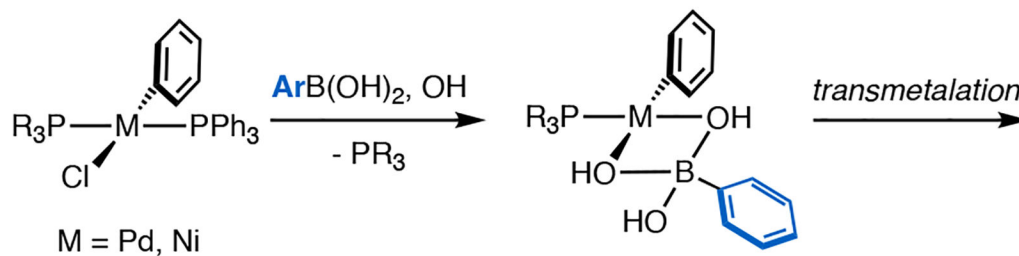


### a. Job plot analysis of reaction 5



maximum observed at mole fraction of 0.5 corresponds to **1:1 Ni to ligand stoichiometry** at the turnover limiting step

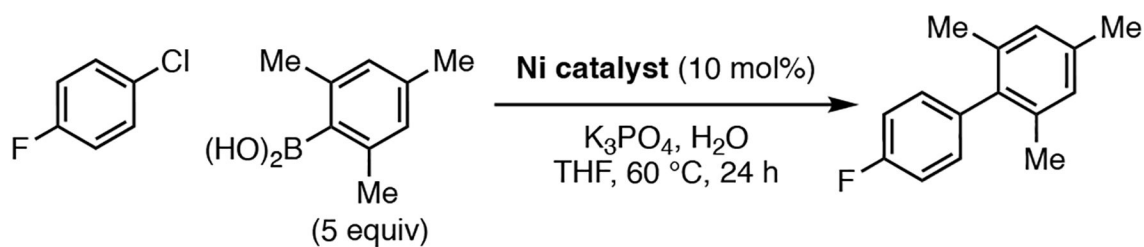
### b. Proposed pre-transmetalation intermediates



Formation requires **ligand dissociation** to enable two-point binding of boronate

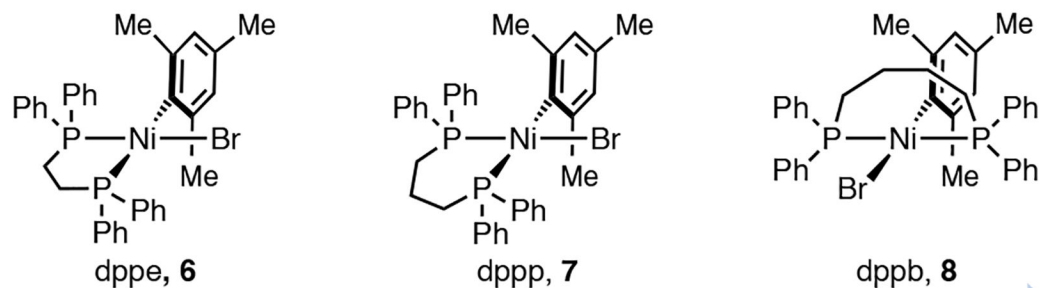
**Figure 6.**

**a.** Job plot analysis of reaction 5. Rates were determined by initial rates, monitoring product formation by  $^{19}\text{F}$  NMR as a function of time against a 2-fluorobiphenyl internal standard. Runs performed in duplicate. See Supporting Information for full procedures. **b.** Pre-transmetalation intermediates. Ligand dissociation is required to enable the two-point binding of the hydroxyboronate species, which is supported by the Job plot analysis.



ligand	geometry	yield (%) precatalyst	yield (%) $Ni(COD)_2 + L$
dppe	<i>cis</i>	0	2
dppp	<i>cis</i>	3	3
dppb	<i>trans</i>	24	54

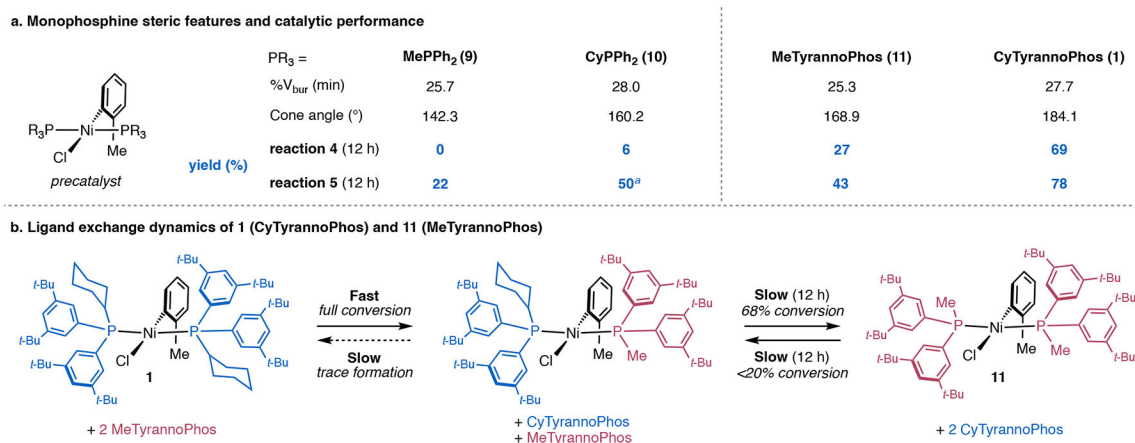
Precatalysts:



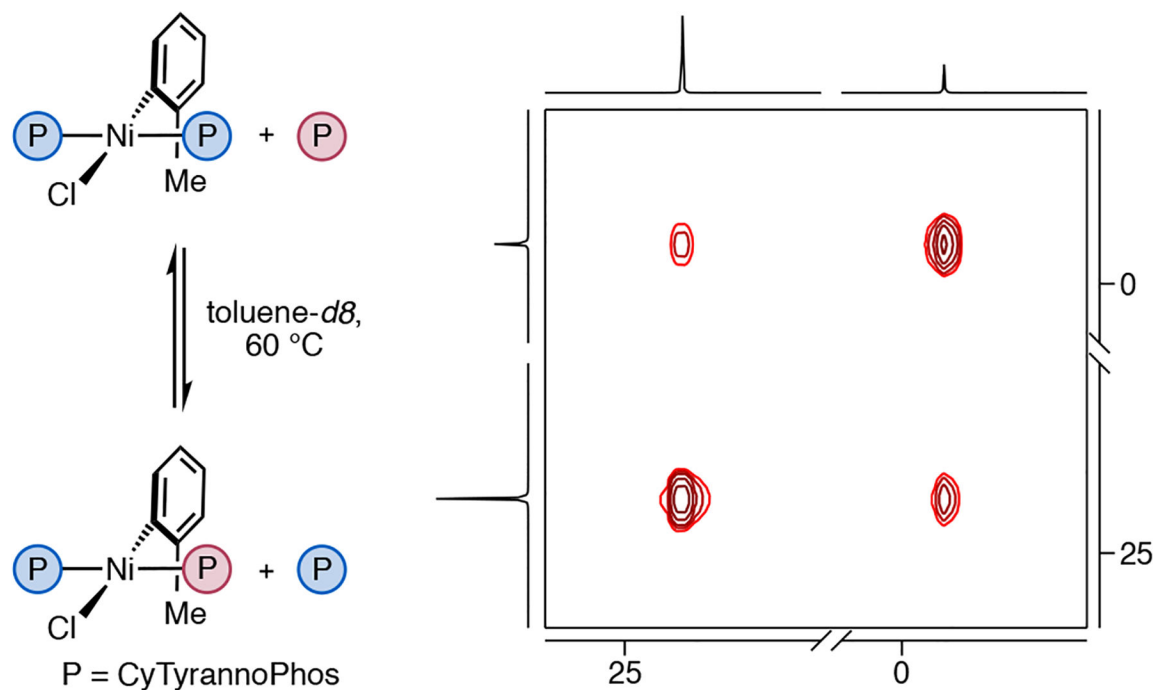
increasing ligand flexibility, increasing reaction yield

**Figure 7.**

**Reaction 5** yields as a function of bisphosphine linker length. Yields determined by  $^{19}F$  NMR analysis against a 1-fluoronaphthalene external standard. Unless otherwise indicated, conditions were identical to those in Figure 3. See Supporting Information for synthesis and characterization of the precatalyst complexes.

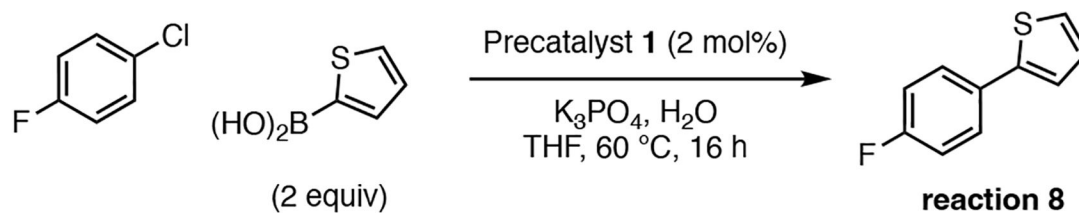
**Figure 8.**

**a.** Monophosphine reactivity in **reactions 4** and **5**. Ligand steric features were determined by computational methods as detailed in reference 22.<sup>22</sup> The cone angle value shown is the Boltzmann average value. Yields determined by <sup>19</sup>F NMR analysis against a 1-fluoronaphthalene external standard. Unless otherwise indicated, conditions were identical to those in Figure 3. **b.** Ligand exchange with CyTyrannoPhos and MeTyrannoPhos. Progress of each species was monitored by <sup>31</sup>P NMR. Performed in C<sub>6</sub>D<sub>6</sub> (0.007M) at room temperature. <sup>a</sup>Run using Ni(COD)<sub>2</sub> and CyPPh<sub>2</sub>



Rate of ligand exchange *unaffected* by change in ligand concentration

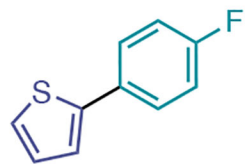
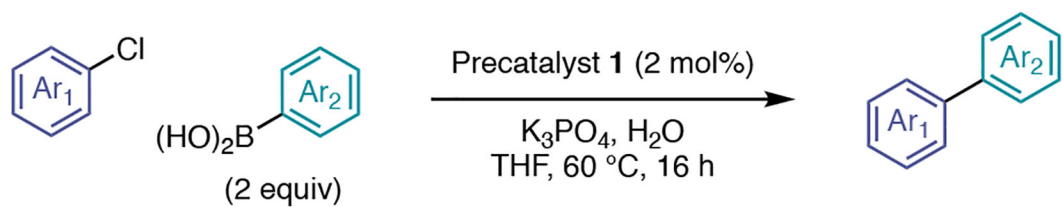
**Figure 9.**  $^{31}\text{P}$  2D EXSY of  $(\text{CyTyranPhos})_2\text{Ni}(o\text{-tolyl})(\text{Cl})$  (**1**) in toluene- $d_8$  at 60 °C ( $t_m = 2.5$  s). The peak at 23.7 ppm corresponds with **1**, with the free ligand at  $-0.95$ .



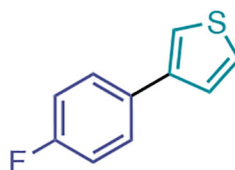
Entry	Deviation	Yield (%)
1	none	33
2	1 equiv. thiophene	17
3	2 equiv. thiophene	10
4	5 equiv. boronic acid	16
5	1 equiv. boronic acid	56
6	1 equiv. 2-phenyl-thiophene	30

**Figure 10.**

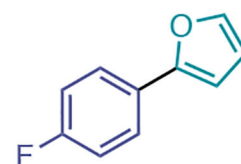
Reactivity of **1** with 2-thiophenylboronic acid. Yields determined by  $^{19}\text{F}$  NMR analysis against a 1-fluoronaphthalene external standard. Unless otherwise indicated, conditions were identical to those in Figure 3. See Supporting Information for full experimental details.



reaction 9  
90% yield



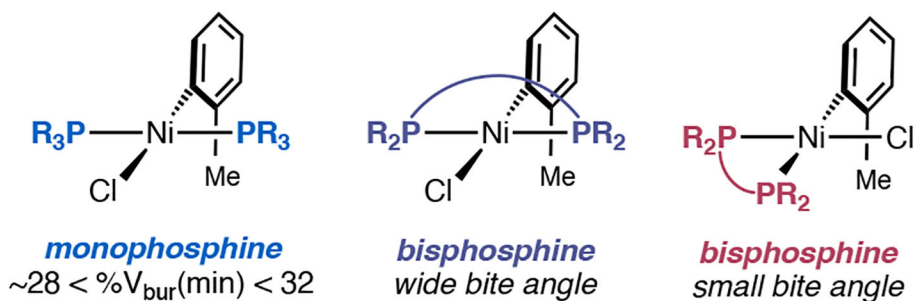
reaction 10  
80% yield



reaction 11  
98% yield

**Figure 11.**

Reactivity of **1** with heteroaromatic substrates. Yields determined by <sup>19</sup>F NMR against 1-fluoronaphthalene as an external standard and presented as the average of two runs. Unless otherwise indicated, conditions were identical to those in Figure 3.

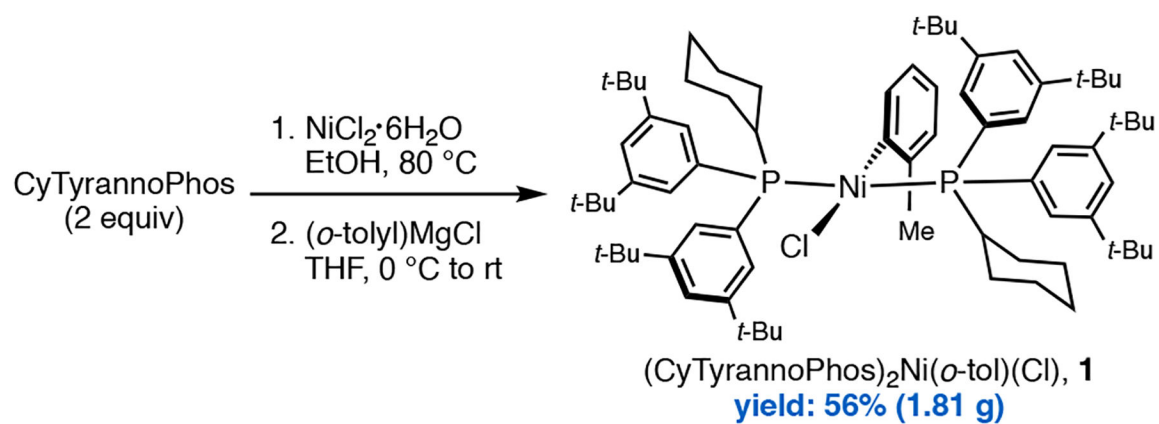


**general substrate guidelines**

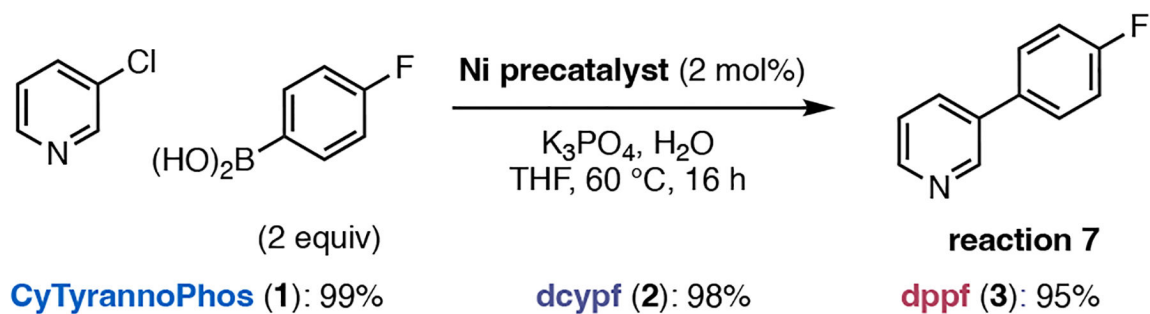
	e-rich and -poor; sterically-hindered; heteroaromatic	e-rich and -poor; sterically-hindered	e-rich and -poor
	e-poor; sterically- hindered	e-rich; sterically-hindered; heteroaromatic	e-rich; heteroaromatic

**Figure 12.**  
 Guidelines for ligand selection across different substrate classes.





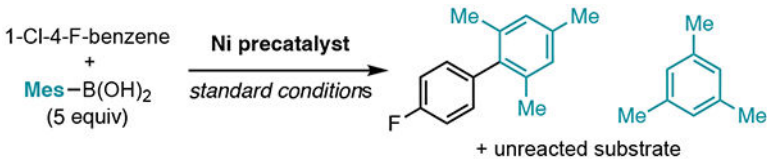
**Scheme 1.**  
Synthesis of monophosphine precatalyst **1**.

**Scheme 2.**Precatalyst reactivity with 3-chloropyridine<sup>a</sup>

<sup>a</sup> Yields determined by <sup>19</sup>F NMR against a 1-fluoronaphthalene external standard and presented as the average of two runs. Unless otherwise indicated, conditions were identical to those in Figure 3.

**Table 1.**

Protodeboronation side products formed in **reaction 5** for reactions catalyzed by **1** and **2**. Mesitylene side product quantified by GC analysis against dodecane internal standard. Remaining boronic acid is not visible by GC after workup. See Supporting Information for full details.

			
Yield (%)			
Precatalyst	Time (h)	Product	Mesitylene
<b>CyTyrannoPhos (1)</b>	12	78	<b>109</b>
	18	86	<b>139</b>
	24	95	<b>143</b>
<b>dcypf (2)</b>	12	90	<b>25</b>
	18	96	<b>29</b>
	24	96	<b>37</b>